Inorganic Chemistry

Article

pubs.acs.org/IC

Density Functional Theory Study of Oxygen-Atom Insertion into Metal−Methyl Bonds of Iron(II), Ruthenium(II), and Osmium(II) Complexes: Study of Metal-Mediated C−O Bond Formation

Daniel B. Pardue,[†] Jiajun Mei,[‡] Thomas R. Cundari,*[,†] and T. Brent Gunnoe*[,‡]

[†]Department of Chemistry, Center for Advanced Scientific Computing and Modeling (CASCaM), University of North Texas, Denton, Texas 76203, United States

[‡]Department of Chemistry, University of Virginia, McCormick Road, P.O. Box 400319, Charlottesville, Virginia 22904-4319, United States

Supporting Information

ABSTRACT: Metal-mediated C−O bond formation is a key step in hydrocarbon oxygenation catalytic cycles; however, few examples of this reaction have been reported for low-oxidation-state complexes. Oxygen insertion into a metal−carbon bond of Cp*M(CO)(OPy)R (Cp* = η^5-pentamethylcyclopentadienyl; R = Me, Ph; OPy = pyridine-*N*-oxide; M = Fe, Ru, Os) was analyzed via density functional theory calculations. Oxygen-atom insertions through a concerted single-step organometallic Baeyer−Villiger pathway and a two-step pathway via a metal−oxo intermediate were studied; calculations predict that the former pathway was lower in energy. The results indicated that functionalization of M−R to M−OR (R = Me, Ph) is plausible using iron(II) complexes. Starting from Cp*Fe(CO)(OPy)Ph, the intermediate Fe−oxo showed oxyl character and, thus, is best considered an $Fe^{III}O^{\bullet-}$ complex. Oxidation of the π-acid ancillary ligand CO was facile. Substitutions of CO with dimethylamide and NH_3 were calculated to lower the activation barrier by ∼1−2 kcal/mol for formation of the $Fe^{III}O^{\bullet-}$ intermediate, whereas a chloride ligand raised the activation barrier to 26 kcal/mol from 22.9 kcal/mol.

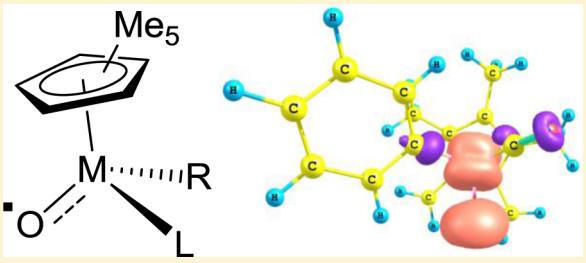

INTRODUCTION

The conversion of hydrocarbons to oxygenated products forms one foundation of the chemical industry. However, many existing processes for oxygenation of hydrocarbons occur at high temperatures and pressures.[1−3] For example, methanol is more desirable than methane because it can be more easily stored and transported, can be used as a fuel or blended with gasoline, and is a precursor to ethylene and propylene.[4] Currently, there is an estimated 2500 trillion ft^3 of natural gas in U.S. reserves.[5] However, in part because of the expense of transportation and distribution of natural gas, disposal by burning (flaring) remains relatively common.[4,6] An efficient method to directly convert methane to methanol (MTM) at ambient temperatures (∼200 °C) and pressures (<500 psi) using dioxygen as the oxidant (either directly or indirectly) remains one of the most desirable chemical transformations, and the selective direction partial oxidation of other hydrocarbons at ambient conditions also would be beneficial.[2,3,7−9]

The current method for conversion of natural gas (of which methane is the primary component) to methanol involves the initial production of syngas (CO/H_2) with a high-temperature (∼800 °C) and -pressure (500 psi) steam reforming catalyst; syngas is then transformed into methanol or other products.[10] The high temperatures and pressures of the two-step process result in prohibitively high capital costs for plants that utilize such chemistry, which thus limit the scaled-up conversion of natural gas to liquids, particularly at remote locations. Efficient low-temperature (<250 °C) and low-pressure direct partial oxidation of methane (and other light alkanes) would provide a less expensive alternative to the two-step process.[2,3,11−13]

Given the strict requirements for selectivity for a viable commercial process for MTM,[3,14] a substantial challenge for partial oxidation of hydrocarbons is the functionalization of strong hydrocarbon C−H bonds in the presence of the weaker C−H bonds of the products. The bond dissociation energy (BDE) of methane C−H bonds is 105 kcal/mol, while the C−H BDE of methanol is 96 kcal/mol.[15] Examples of transition-metal-mediated activation of C−H bonds that are selective (kinetic and thermodynamic) for strong C−H bonds over weaker C−H bonds have been reported.[16−21] Thus, the use of transition-metal catalysts for MTM (and other hydrocarbon oxidations) has been heavily pursued. Electrophilic catalysts based on late transition metals have been among the most successful.[12,22−28] For these catalysts, the carbon-heteroatom bond-forming step is generally proposed to occur by the addition of a nucleophile to an electrophilic alkyl ligand (methyl if the substrate is methane). Thus, the electronegative

Received: November 4, 2013
Published: February 26, 2014

character of the metal is a key feature of these catalysts. Success of this class of catalysts has been limited by product inhibition, slow rates, and the required use of strongly acidic solvents (e.g., concentrated sulfuric acid).

More electron-rich metals [e.g., iridium(I), iridium(III), rhodium(I), rhenium(I), ruthenium(II), iron(II)] are known to initiate C−H activation;[29−36] however, these metals are less likely to have M−R bonds polarized toward electrophilic hydrocarbyl ligands. One method that has received interest involves the development of a catalyst that mediates oxygen-atom insertion into a M−R bond after C−H activation (Scheme 1).[37−51]

Scheme 1. Proposed Catalytic Cycle for Alkane-to-Alcohol Catalysis[a]

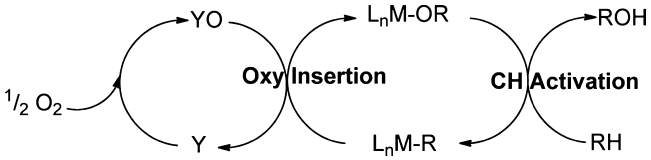

[a]RH = alkane, YO = oxidant, Y = leaving group, and L_nM = catalyst.

There are two key steps in the catalytic cycle for hydrocarbon oxidation shown in Scheme 1: C−H activation via net 1,2-addition across M−OR[52] and C−O (or C−X, where −X can be converted to −OH) bond formation. Although C−H activation is generally regarded as the most challenging step,[2,3,11−13,29−31] well-defined oxy insertion into M−R bonds has less precedent.[2,3,11,12,39−41,45−47] Methyltrioxorhenium (MTO) and $ArReO_3$ (Ar = Ph) react with oxidants to form methanol or a phenol, respectively.[42−45,53,54] Experimental and computational studies suggested that the reactions proceed via a pathway that is similar to an organic Baeyer−Villiger (BV) reaction as opposed to hydrocarbyl migration to an oxo ligand. Our groups have reported that the reaction of Cp*W(O)$_2$(CH_2SiMe_3) with a variety of oxygen-atom donors results in oxy insertion to ultimately form Me_3SiCH_2OH.[46] Mechanistic studies allowed the elucidation of two pathways: one pathway involves a direct oxygen-atom insertion into the W−CH_2SiMe_3 bond, while the second pathway occurs via an η^2-peroxide intermediate. Bercaw and co-workers reported a study of Cp*$_2$Ta(η^2-O_2)CH_3 that showed acceleration of oxy insertion by Lewis and Brønsted acids.[55] Hillhouse and co-workers reported examples of Ni d^8 systems undergoing net oxy insertion into Ni−C bonds using N_2O as the oxidant.[38,41] Very few examples of using a 3d metal to mediate oxy insertion into a metal−carbon bonds are known, but calculations suggest that such transformations could occur with low activation barriers.[47] Figg and Cundari studied the mechanism of the Hillhouse system.[39] Our current research aims to extend the aforementioned studies to (a) different transition-metal systems (particularly those incorporating Earth-abundant 3d metals), (b) complexes with metals in non-d^0 electronic configurations (because these are most likely to combine oxy insertion with C−H activation), (c) a variety of oxidants, particularly mild oxidants, and, most importantly, dioxygen, (d) organometallic motifs demonstrated to effect C−H activation to expand the knowledge base for oxy insertion (M−R → M−OR) and to identify viable catalysts for hydrocarbon partial oxidation.[45]

Recently, a joint experimental and computational analysis of aromatic C−H activation by Cp*Fe(CO)(NCMe)Ph (Cp* = pentamethylcyclopentadienyl) under ambient conditions has been reported.[35] This work set the foundation for efforts to uncover inexpensive catalysts for partial hydrocarbon oxidation. Theory in concert with experiment indicates a preferred C−H activation pathway for Cp*Fe(CO)Ph involving σ-bond metathesis, which maintains iron in the Fe^{II} oxidation state. Hence, subsequent oxy-insertion steps may still access reasonably available $Fe^{III/IV}$ states even if a nonredox, BV pathway presents a high activation barrier. Also, analyses suggested that formally spin-forbidden processes, long a concern in 3d metal catalysis, did not hinder the C−H activation transformations.[56,57] In another important experimental precedent, Ni and Power[58] have reported oxy functionalization of coordinatively unsaturated iron(II) aryls utilizing dioxygen as the oxidant.

Given these recent reports of C−H activation/functionalization and C−O bond formation using iron(II) complexes, we sought to undertake a modeling study of oxy-insertion reactions relevant to the iron(II) complex Cp*Fe(CO)(NCMe)Ph and heavier group 8 congeners. In the present paper, the results of a computational study are reported for redox (i.e., formation of metal−oxo intermediates) versus organometallic BV (OMBV; no change in the metal formal oxidation state) pathways for oxy insertion by CpM^{II}(CO)R (M = Fe, Ru, Os). The goal of this work is not to design a new experimental complex capable of oxy insertion per se but to gain insight into the challenges that must be overcome when designing an experimental complex that is capable of accomplishing oxy insertion. The primary goals of this research are to (1) compare redox versus nonredox pathways for oxy insertion and (2) identify the key electronic features of iron(II) complexes that define the potential energy surfaces for oxy insertion.

COMPUTATIONAL METHODS

Density functional theory (DFT) within the *Gaussian09* package[59] was used for geometry optimization and vibrational frequency calculations. A standard level of theory was employed: B3LYP or M06 with a double-ζ basis set with pseudopotentials and added d functions for main-group elements [e.g., CEP-31G(d)].[60] This level of theory has been used in previous modeling of oxygen-atom transfer and oxy-insertion reactions and was shown to correspond well with experimental trends while maintaining reasonable computational cost.[37,39,46,47] Tests with larger basis sets were also performed and shown to negligibly impact the potential energy surfaces of interest. The reader should assume a B3LYP/CEP-31G(d) level of theory, unless otherwise stated. Calibration of the various theoretical components (functional, basis sets, solvent, etc.) is discussed in the Supporting Information.

The energies quoted are free energies that were calculated at 298.15 K and 1 atm. The stationary points were defined as minima or transition states (TSs) by the presence of 0 or 1 imaginary frequencies, respectively, as obtained from the calculated energy Hessians. Different spin states were studied for the 3d metals; the 4d and 5d systems were all calculated to be singlets in their lowest-energy states with the exception of the Ru^{IV}−oxo intermediate structure, which was predicted to be a triplet.

RESULTS AND DISCUSSION

Modeling of the oxygen-atom insertion reactions begins with Cp*Fe(CO)(OPy)Ph (**1**), where Py = pyridine and Cp* = η^5-C_5Me_5. The metallo-Criegee intermediate (MCI), Cp*Fe(CO)(OPy)Ph, named using the language of the organic BV reaction,[61] is the adduct formed upon coordination of the oxidant (e.g., pyridine-*N*-oxide) to the 16-electron complex Cp*Fe(L)Ph. We have calculated the energetics for oxygen-

dx.doi.org/10.1021/ic402759w | Inorg. Chem. 2014, 53, 2968−2975

atom insertion into the Fe−Ph bond of **1** by the OMBV pathway and via formation of an Fe−oxo complex. To understand the roles that the metal identity, ancillary ligands, and oxidant play, substitutions were made at various positions in the MCI Cp*M(R)(OY)(L): M = Fe, Ru, Os; YO = OPy, 4-NO_2-OPy, 4-NMe_2-OPy; L = CO, NO^+, Cl^-, NMe_2^-, NH_3; R = C_6H_5, *m*- and *p*-NO_2-C_6H_5, *m*- and *p*-NMe_2-C_6H_5) and the energetics for oxygen-atom insertion were calculated (Chart 1).

Chart 1. Series of Complexes Studied

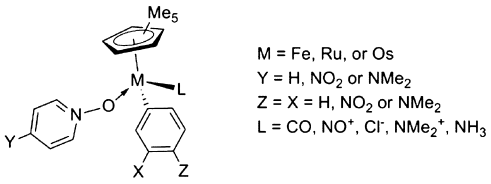

BV Mechanism for Oxy Insertion: Cp*Fe(Ph)(OPy)(CO). The OMBV pathway for oxy insertion into the Fe−Ph bond of **1** is shown in Scheme 2. Pyridine is released from the

Scheme 2. B3LYP/CEP-31G(d)-Calculated Reaction Pathway for the OMBV Transformation of 1 to Cp*Fe(CO)(Py)OPh[a]

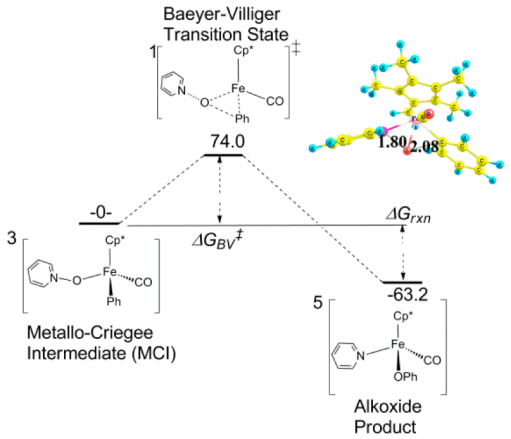

[a]The lowest-energy spin state is denoted by a prefix numeral. Free energies (standard temperature and pressure) are given in kcal/mol relative to the MCI. The calculated BV TS structure is top right.

PyO oxidant in concert with insertion of the oxygen atom into the Fe−Ph bond.[37,45,47] The B3LYP/CEP-31G(d)-optimized geometry of the singlet BV TS is given in Figure S1 (Supporting Information, SI) and is similar to OMBV TSs reported previously.[37,44−47,54] At the B3LYP/CEP-31G(d) level of theory, formation of the phenoxide product is highly exergonic by −63.2 kcal/mol, but the OMBV conversion of Cp*Fe(Ph)(OPy)(CO) to Cp*Fe(OPh)(Py)(CO) has a prohibitively large calculated free-energy barrier of $\Delta G_{BV}^{\ddagger}$ = 74.0 kcal/mol (Scheme 2). The OMBV TSs for triplet and quintet multiplicity could not be found, despite numerous starting geometries and TS searches. In each case, the high-spin TSs converged to previously identified stationary points. This is perhaps not surprising because the strongly π-acidic CO ligand will stabilize low-spin complexes. As discussed more fully in the SI, these preliminary studies led us to focus in this manuscript on a two-step pathway via an Fe−oxo intermediate for the overall oxy-insertion reaction.

Oxo Pathway: Impact of Metal. Periodic trends for oxy insertion by the Fe−oxo pathway were probed for Cp*M(CO)(OPy)Ph (M = Fe, Ru, Os; Scheme 3). The overall oxy

Scheme 3. B3LYP/CEP-31G(d)-Calculated Formation of Oxo Intermediate and Phenyl Migration Steps in the Redox Pathway for Oxy Insertion Comparing Energetics for Group 8 Metals[a]

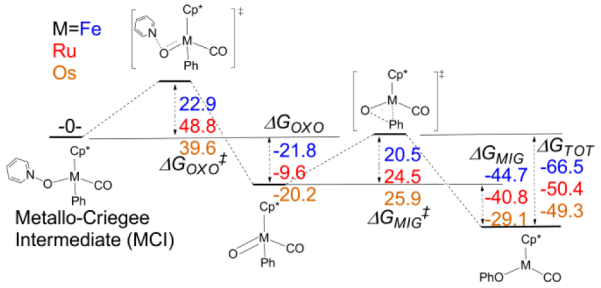

[a]Calculated relative and absolute free energies (kcal/mol), Cp*M(OPy)(CO)(Ph), for iron (blue), ruthenium (red), and osmium (orange).

insertions from Cp*M(CO)(OY)Ph to make the phenoxide complexes Cp*M(CO)OPh (ΔG_{tot}) were calculated to become less exergonic for the heavier metals: −66.5 (Fe), −50.4 (Ru), and −49.3 (Os) kcal/mol. All Ru and Os ground states were calculated to be singlets with the exception of the Ru^{IV}−oxo intermediate Cp*Ru(CO)(O)Ph, which is predicted to be a triplet. In all three cases, formation of the oxo was exergonic relative to the MCI: ΔG_{oxo} (kcal/mol) = −21.8 (Fe), −9.6 (Ru), and −20.2 (Os) (Scheme 3). The free-energy barrier for formation of the oxo complex Cp*M(CO)(O)Ph ($\Delta G_{oxo}^{\ddagger}$) is calculated to be substantially lower for the iron complex (22.9 kcal/mol) than for ruthenium (48.8 kcal/mol) or osmium (39.6 kcal/mol). The overall $\Delta\Delta G_{oxo}^{\ddagger}$ (>25.9 kcal/mol) indicates that the first-row metal iron has a tremendous kinetic advantage for oxidation to the metal−oxo intermediate. $\Delta G_{oxo}^{\ddagger}$ does not appear to be dictated by the thermodynamics of metal−oxo formation because ΔG_{oxo} is most favorable for iron and osmium (both exergonic by >20 kcal/mol) than ruthenium (ΔG_{oxo} = −9.6 kcal/mol). The lower activation barrier for iron seems surprising because more facile oxidation of ruthenium and osmium compared to iron might be anticipated. The different geometries of the group 8 triad can be seen in Figure 1. The M−O bond length in Cp*M(CO)(OPy)Ph is ∼0.1 Å shorter for M = Fe than that for M = Ru and Os. Constrained geometry calculations on PyO suggest that this perturbation has a free-energy cost of ∼4 kcal/mol, which provides partial reasoning

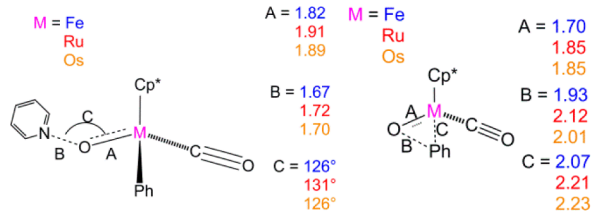

Figure 1. B3LYP/CEP-31G(d)-calculated bond lengths (Å) and bond angles (deg) of the TS active sites for different group 8 metals for the TSs for formation of oxo complexes (left) and for phenyl-to-oxo migration (right).

dx.doi.org/10.1021/ic402759w | Inorg. Chem. 2014, 53, 2968−2975

why the barrier concerning M = Fe is lower than that of M = Ru and Os.

Although hydrocarbyl migration to an oxo ligand has been considered a challenging reaction,[48,62,63] for all three Cp*M(CO)(O)Ph complexes, the calculated free energy of activation for phenyl migration to the oxo ligand is lower than the corresponding activation energy for formation of the oxo complex ($\Delta G_{oxo}^{\ddagger}$). Thus, the rate-limiting step is predicted to be formation of the metal−oxo intermediate. The intermediate Cp*Fe(CO)(O)Ph possesses oxyl character as opposed to oxo (see the SI). For phenyl migration to the oxo ligand, the iron complex is predicted to hold a kinetic advantage over ruthenium and osmium complexes, but $\Delta\Delta G_{mig}^{\ddagger}$ (5.4 kcal/mol) is less than $\Delta\Delta G_{oxo}^{\ddagger}$ (25.9 kcal/mol). Because the geometric differences for the metal−oxo complexes and the TSs for phenyl migration are small (see below and Figure 1), it is likely that the larger $\Delta G_{mig}^{\ddagger}$ values for ruthenium and osmium result from the stronger metal−oxo π bonds for the heavier metals. Thus, weaker metal−oxo bonding is expected to facilitate hydrocarbyl migration to the oxo π ligand. Perhaps important is that this rationale differs from that proposed by Mayer et al. for their study of phenyl-to-oxo migration for $[TpRe(O)_2Ph]^+$.[48] Suggested therein is that strong π donation, which should increase the metal−oxo bond strength, is vital to impart electrophilicity at the oxo ligand and, in turn, a low barrier for phenyl-to-oxo migration.

Table 1 lists M−O bond distances as well as spin multiplicity for the oxo intermediates of M = Fe, Ru, and Os. Also, the spin densities for M = Fe and Ru (the Os−oxo intermediate is computed to be a ground-state singlet) as well as M = O are listed. Table 1 shows M = Fe to have the shortest $M-C_{Ph}$ bond distance at 0.12 and 0.11 Å longer for M = Ru and Os, respectively.

Table 1. Comparison of the M=O Bond Lengths, Bond Angles, Spin Densities, M−C Bond Lengths (Ph), M=O Bond Strengths for Cp*M(CO)(O)Ph (M = Fe, Ru, Os), and M−OPy Bond Strength (kcal/mol), [ΔH Values in Parentheses] for Cp*M(CO)(OPy)Ph (M = Fe, Ru, Os)[a]

	Fe	Ru	Os
M=O bond distance (Å)[a]	1.673	1.842	1.799
multiplicity[a]	3	3	1
M spin density (e^-)[a]	1.262	0.784	
O spin density (e^-)[a]	0.923	1.105	
$M-C_{Ph}$ (Å)[a]	1.998	2.119	2.106
M=O BDFE[a,b]	60.1	60.8	68.2
∠M−O−N (deg)[c]	121.2	128.9	128.7
M−OPy BDFE[b,c]	−5.5 (4.6)	7.4 (19.8)	4.2 (16.7)

[a]For Cp*M(CO)(O)Ph. [b]In kcal/mol. [c]For Cp*M(CO)(OPy)Ph. [a]Structures calculated at the B3LYP/CEP-31G(d) level of theory.

Computed $\Delta G_{oxo}^{\ddagger}$ and ΔG_{oxo} values were compared for B3LYP and M06 functionals for group 8 metals (Table 2). The M06 functional makes formation of the oxo consistently less exergonic by ca. 7 kcal/mol. Interestingly, the impact of the functional is less systematic for the activation barrier, raising one (osmium) and lowering the other (ruthenium) barrier relative to iron. B3LYP was used herein given its utility in previous studies of 3d metal oxy insertion,[37,39,46,47] although the present work suggests that further calibration may be prudent for studies of similar 4d and 5d reactions.

Table 2. Comparison of the B3LYP and M06 Functionals, Both Computed with the CEP-31G(d) Basis Set

method	metal	$\Delta G_{oxo}^{\ddagger}$	ΔG_{oxo}
B3LYP	Fe	22.9	−21.8
M06	Fe	28.9	−16.3
B3LYP	Ru	48.8	−9.6
M06	Ru	29.5	0.1
B3LYP	Os	39.6	−20.2
M06	Os	48.3	−12.2

The computed M−OPy bond dissociation free energy (BDFE) of Cp*M(CO)(OPy)Ph complexes is exergonic (−5.5 kcal/mol; ΔH = 4.6 kcal/mol) for M = Fe and endergonic, 7.4 kcal/mol (ΔH = 19.8 kcal/mol) and 4.2 kcal/mol. (ΔH = 16.7 kcal/mol), for M = Ru and Os, respectively.

Given the similar ground-state and TS structures (Figure 1), we propose that binding of OPy to the larger metal is facilitated by more favorable steric factors especially given the bent coordination of ligated pyridine-*N*-oxide (see ∠M−O−N in Table 1). The BDFEs for oxidant binding suggest that a major contribution to the differences in $\Delta G_{oxo}^{\ddagger}$ between iron and its heavier congeners could be stabilization of the ground-state energies upon coordination of OPy for the ruthenium and osmium complexes relative to iron.

Impact of the Migrating Group: Replacement of Phenyl with Methyl. Because conversion of alkanes is a primary target for catalytic oxidation reactions, the impact of replacing the phenyl ligand of **1** with methyl to give Cp*Fe(CO)(OPy)Me was studied. The free-energy barrier to oxo formation ($\Delta G_{oxo}^{\ddagger}$) was lowered by 1.3 kcal/mol for the methyl complex compared to the phenyl complex (Scheme 4),

Scheme 4. Reaction Pathway Comparing R (Phenyl vs Methyl)[a]

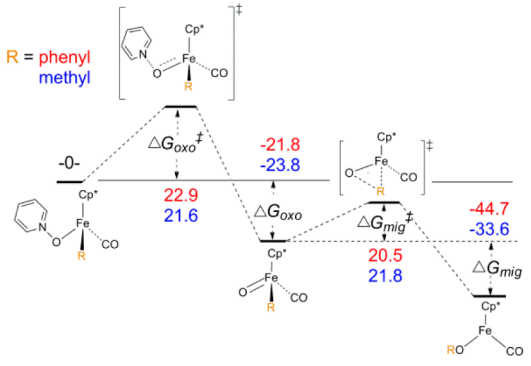

[a]Free energies are listed (kcal/mol) relative to the MCI. Calculated at the B3LYP/CEP-31G(d) level of theory.

and formation of the oxo (ΔG_{oxo}) is calculated to be more exergonic by 2.0 kcal/mol. The modest changes in ΔG_{oxo} and $\Delta G_{oxo}^{\ddagger}$ are reasonable because the hydrocarbyl group is a spectator ligand in the formation of the oxo intermediate.

For the second step of the overall oxy-insertion reaction, the free-energy barrier for methyl migration ($\Delta G_{mig}^{\ddagger}$) was calculated to be 21.8 kcal/mol for the methyl derivative (Scheme 4) versus 20.5 kcal/mol for the corresponding phenyl complex. The higher barrier for methyl versus phenyl migration is consistent with previous calculations on platinum(II) complexes.[37] For organic oxy-insertion transformations, phenyl migration is more facile than methyl migration,[37,64] so the

dx.doi.org/10.1021/ic402759w | Inorg. Chem. 2014, 53, 2968−2975

calculated larger activation barrier for methyl migration to the oxo ligand is not surprising; however, the relatively modest $\Delta\Delta G_{mig}^{\ddagger}$ of 1.3 kcal/mol is smaller than anticipated[61] (see below) and bodes well for the development of catalysts for methane functionalization. Moreover, unlike previous studies of OMBV insertion of second- and third-row transition metals,[37,47,65] the calculated free-energy barriers for methyl migration from Cp*Fe(CO)(O)Me are reasonable for incorporation into catalytic cycles. In the present case, the methyl migration TS lies below the free energy of the initial oxo formation TS, so that the latter is still calculated to be the rate-limiting step in the overall oxy-insertion process.

Given the small $\Delta\Delta G_{mig}^{\ddagger}$ of 1.3 kcal/mol for phenyl and methyl migration, we sought to probe whether radical processes might compete with concerted hydrocarbyl migration. The data in Table 3 provide a comparison of the calculated BDFEs for

Table 3. Comparison of Calculated BDFEs (kcal/mol) to Free Energies of Activation for Hydrocarbyl Migration to Oxo Ligands ($\Delta G_{mig}^{\ddagger}$, kcal/mol)

	BDFE		$\Delta G_{mig}^{\ddagger}$
Fe−Me	9.8	<	21.8
Fe−Ph	19.6	≈	20.5

Fe−Me and Fe−Ph of Cp*Fe(CO)(O)(R) (R = Me or Ph) to the free-energy barriers for phenyl and methyl migration ($\Delta G_{mig}^{\ddagger}$). The computed BDFE for the Fe−Me bond is substantially lower (by 12 kcal/mol) than the calculated barrier for migration of the methyl, and the Fe−Ph BDFE is calculated to be more similar to the free-energy barrier for phenyl migration and within the limits of uncertainty of the computational methods. On the basis of these data, it is reasonable to assume that homolytic cleavage of the Fe−Me ligand to form a methyl radical might compete with the even-electron concerted migration. Of course, formation of a radical methyl could be followed by rapid rebound to the oxo ligand to form a C−O bond.[66−68] In contrast to the Fe−Me intermediate, the calculated energetics for the Fe−Ph complex suggest that a migration route to form the phenoxide ligand is likely to be competitive with a radical pathway. Hammett studies (see the SI) of the migration of *p*-C_6H_4X (X = NO_2, H, NMe_2) yielded small $\Delta\Delta G^{\ddagger}$ values (<2 kcal/mol) and thus may also be interpreted to imply radical character in the oxy-insertion transformations, and thus limited charge buildup in the hydrocarbyl group, in the migrating step for iron. Such considerations are important for catalyst design because competition between the even- and odd-electron pathways is a well-known challenge in utilizing Earth-abundant 3d metals in catalysis. To achieve selective catalysts, avoiding radical transformations may be desirable.

C−H Activation. The focus of this work is on oxy insertion within the catalytic cycle for hydrocarbon-to-alcohol conversion. However, to complete a model catalytic cycle for MTM, the C−H activation step was calculated. As can be seen in Scheme 5, coordination of methane to Cp*Fe(CO)(OCH_3) is endergonic by 6.4 kcal/mol. The calculated free energy of activation for 1,2-CH-addtion of methane across the Fe−OMe bond of Cp*Fe(CO)(OCH_3) is 47.2 kcal/mol, with the product Cp*Fe(CO)($HOCH_3$)(CH_3) being endergonic by 37.3 kcal/mol. While these model complexes may have high barriers, related Cp*Fe complexes activate aromatic C−H bonds.[35,36] The presence of a π-donating ligand, such as

Scheme 5. Reaction Pathway Showing CH Activation Energies[a]

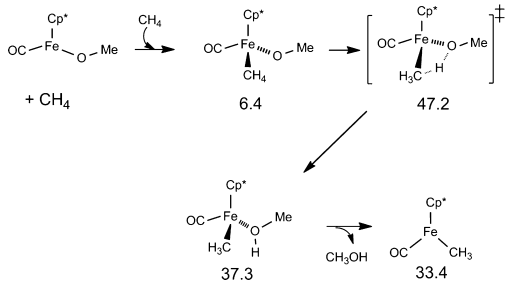

[a]Free energies are listed (kcal/mol) relative to the separated reactants, i.e., Cp*Fe(CO)(OCH_3) + CH_4. Calculated at the B3LYP/CEP-31G(d) level of theory.

methoxide, has been predicted by calculations to increase activation barriers.[69]

Effect of Ligand L for Cp*Fe(L)(OPy)Ph Complexes. The role of the ancillary ligand L of Cp*Fe(L)(OPy)Ph complexes was studied. The CO in **1** was replaced with four different ligands: NO^+, Cl^-, NMe_2^-, and NH_3 (Scheme 6). The

Scheme 6. B3LYP/CEP-31G(d)-Calculated Energetics (kcal/mol) for Fe−Oxo Formation and Phenyl-to-Oxo Migration for Cp*Fe(L)(OPy)Ph Complexes

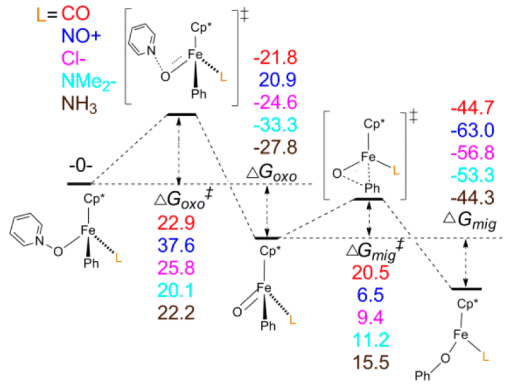

overall charge of the complex was adjusted to maintain a formal Fe^{II} oxidation state for the starting complex. As shown in Scheme 6, when CO is replaced with NO^+, the free-energy barrier for formation of the Fe−oxo complex is calculated to increase by 14.7 kcal/mol. Likewise, the presence of the nitrosyl ligand results in a large change in the thermodynamics, rendering the formation of the oxo complex endergonic by nearly 21 kcal/mol, which is a $\Delta\Delta G_{oxo}$ of >40 kcal/mol compared to the CO complex. Given the similar properties of isoelectronic CO and NO^+ (i.e., both are strong π acids), the large increases in $\Delta G_{oxo}^{\ddagger}$ and ΔG_{oxo} are likely a result of the positive charge associated with by the nitrosyl ligand. The formation of a high-oxidation-state Fe−oxo intermediate likely is disfavored by the overall positive charge. For the chloride and amide ligands, the computed activation barriers for oxo formation are similar to the CO complex with a slight increase of ~3 kcal/mol for chloride and a decrease of ~2 kcal/mol for the amide ligand. Thus, overall anionic complexes do not exhibit a general positive benefit. The decrease in the activation barrier for the amide ligand could indicate a positive role for π-donating ligands. Replacing the strong π acid CO with NH_3, a charge neutral ligand and σ donor, results in a very modest

dx.doi.org/10.1021/ic402759w | Inorg. Chem. 2014, 53, 2968−2975

change of 0.7 kcal/mol for the activation barrier for Fe−oxo formation. Taken together, the data suggest that the overall charge of the complex is likely to be more important than the relative σ/π-donor/acceptor profile of the ancillary ligand for the formation of Fe−oxo complexes from Cp*Fe(L)(OPy)R complexes. Whether this is a general trend for other iron(II) and d^6 metal complexes is unclear.

The free-energy barriers for phenyl migration ($\Delta G_{mig}^{\ddagger}$) for the Cp*Fe(L)(OPy)Ph complexes were found to vary substantially (Scheme 6); however, in all cases, the predicted rate-limiting step remains formation of the Fe−oxo intermediate. The calculated $\Delta G_{mig}^{\ddagger}$ values for L = CO, NO^+, Cl^-, NMe_2^-, and NH_3 are 20.5, 6.5, 9.4, 11.2, and 15.5 kcal/mol, respectively. The migration barrier was lower for all of the coligands considered versus that of the CO.

Acyl Formation. Ison and co-workers have reported remediated C−O bond formation via CO insertion to form an acyl followed by acyl migration to an oxo ligand.[70] Competing migration of the methyl and phenyl ligands to the carbonyl coligand was considered (Scheme 7): Cp*Fe(CO)(O)Ph → Cp*Fe(C(O)R)(O) (R = Me, Ph). The $\Delta G_{acyl}^{\ddagger}$ barriers predict that acyl formation will compete with formation of the alkoxide or aryloxide when the coligand is CO. The acyls bind in a κ^1 manner for both Cp*Fe(C(O)R)(O) structures, i.e., R = phenyl and methyl. The energetics for this side reaction suggest the use of a coligand that would not facilitate this side reaction. The TS for migration of coligand Cl^- to CO could not be isolated.

Scheme 7. Reaction Pathway for R Migration to Carbonyl i.e., Acyl Formation[a]

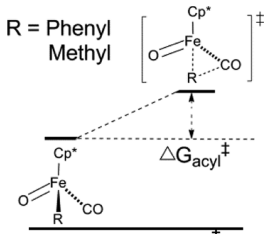

R	$\Delta G_{acyl}^{\ddagger}$
Phenyl	12.9
Methyl	12.7

[a]Free energies are listed (kcal/mol) relative to the oxyl intermediate. Calculated at the B3LYP/CEP-31G(d) level of theory.

Ligand Oxidation. Given the oxidizing conditions for a catalytic process, competing ligand oxidation is an important factor in coligand selection. For example, oxidation of the CO ligand to CO_2 is an obvious concern for the complexes Cp*M(CO)(OPy)R. From the classic review by Holm and Donahue,[71] $Cl^- \rightarrow ClO^-$ has a much less favorable oxygen-atom-transfer potential (ΔG_{aq} = +22.6 kcal/mol) than CO → CO_2 (ΔG_g = −61.5 kcal/mol). In this regard, anionic coligands like chloride and dimethylamide seem promising targets for experimental study.

To probe the energetics of oxygen-atom transfer to ancillary ligands, three complexes were modeled (L = CO, NO^+, Cl^-) on the basis of the barriers associated with formation of the oxo intermediates (Scheme 6). The thermodynamics for oxygen-atom transfer to CO and NO^+ ligands are calculated to be exergonic, while oxidation of chloride is thermoneutral (Scheme 8). The calculated energetics indicated that the L → LO side reaction can be very favorable, as expected, and therefore needs to be considered for catalyst design. The calculations indicate that hard, electronegative coligands like chloride are good synthetic targets.

Scheme 8. B3LYP/CEP-31G(d)-Calculated Energetics (kcal/mol) for Oxygen-Atom Transfer from the Oxo Ligand of Cp*Fe(L)(O)Ph to the Ligands L[a]

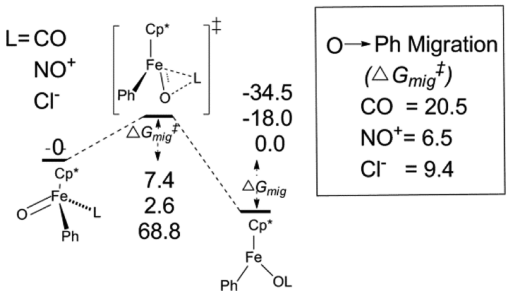

[a]For comparison, the oxygen-to-phenyl migration barriers (see Scheme 6) are also noted.

SUMMARY, CONCLUSIONS, AND PROSPECTUS

Recent conceptual and synthetic achievements have significantly advanced the goal of achieving oxy insertion into M−C bonds.[35,39,46] When combined with the recent experimental demonstration of C−H activation by iron(II) and nickel(II) complexes,[35,39] the goal of selective hydrocarbon functionalization via metal-mediated C−H activation and subsequent M−R functionalization seems viable. The present computational results reveal that the functionalization M−R to M−OR is plausible through the use of iron(II) starting complexes and provides some guidance on experimentally plausible research directions.

Baseline complex **1** was modified to gain insight into the impact of modification of the chemical components on the thermodynamics and kinetics of oxy insertion into the Fe−Ph bond. The main points are as follows:.

(1) Calculations support a two-step (or redox) oxo-mediated pathway as being more energetically favorable in comparison to a one-step (or nonredox) OMBV pathway. Moreover, for the systems modeled here, the initial barrier to oxo formation ($\Delta G_{oxo}^{\ddagger}$ = 22.9 kcal/mol) is marked the highest point on the reaction coordinate, while the TS for phenyl migration is predicted to occur with a lower free energy of activation ($\Delta G_{mig}^{\ddagger}$ = 20.5 kcal/mol).

The oxo intermediate formed by the initial oxygen-atom transfer from OPy to the metal is most accurately described as an oxyl ($Fe^{III}O^{\bullet -}$; see the SI) as opposed to an oxide ($Fe^{IV}O^{2-}$) or oxene ($Fe^{II}O^{\bullet\bullet}$) intermediate. This echoes a recent computational study[39] of oxy insertion into a Ni^{II}−hydrocarbyl bond.[38,41,72] Modification of the supporting ligands to enhance the oxyl identity and the correlation this may have with oxy-insertion activation barriers would be of interest from both an experimental and computational perspective, not only for the current models but also for other systems.[49,72] One may reasonably hypothesize that the reduced nucleophilicity of an oxyl versus an oxide may enhance the hydrocarbyl migration aptitude.

(2) The iron of **1** was replaced by ruthenium and osmium. The barriers for the oxo formation step showed the 3d and 4d metals to be more similar, with osmium having the most divergence. The strength of bonding of the oxidant OPy to

dx.doi.org/10.1021/ic402759w | Inorg. Chem. 2014, 53, 2968−2975

Cp*M(CO)Ph was identified as an important discriminant among the group 8 metals. The barriers for alkyl migration trended as Fe > Ru > Os, which contrasted the calculated trend for the metal−oxo formation step. Thus, as in a previous study of the OMBV mechanism, 3d metals display a computed advantage over their 4d and 5d counterparts. It is reasonable to assume, given the combination of results from this and past[38,39,41,72] research that the weakness of the M−C bond is a major determinant of this trend. The prediction of weaker metal−oxo bonds being more favorable for hydrocarbyl migration is seemingly in contrast to previous work by Brown and Mayer;[48] however, given the oxyl character (see the SI) of the Fe−oxo complex compared to diamagnetic Re^{VII}−oxo complexes, differences in trends are not necessarily surprising.

(3) While the studies of **1** reported herein indicate the viability of oxy insertion into Fe−R bonds, experimental demonstration and extension to catalysis will likely require different supporting ligands less prone to oxidation (i.e., CO and Cp* are likely to be problematic). When considering the L → LO side reaction, the introduction of Cl^- as a coligand showed the most promise.

(4) Substitution of a phenyl with a methyl group in the R position raised the activation barrier for hydrocarbyl-to-oxo migration by only 1.3 kcal/mol. Calculated Fe−C BDFEs imply that Fe−R → Fe−OR transformation may have substantial radical character to it, especially for R = Me. Unlike the phenyl congener, the calculated BDFE for Fe−methyl scission is substantially lower than the activation barrier for migration of the methyl ligand to the oxo ligand. If this radical reactivity could be harnessed, it may overcome one of the major challenges inherent in nonredox BV pathways for oxy insertion, i.e., the extreme reluctance of a nucleophilic methyl to transfer to an oxygen atom.

■ ASSOCIATED CONTENT

Supporting Information

Details of calculations and a full citation for ref 59. This material is available free of charge via the Internet at http://pubs.acs.org.

■ AUTHOR INFORMATION

Corresponding Authors

*E-mail: Thomas.Cundari@unt.edu.

*E-mail: tbg7h@eservices.virginia.edu.

Notes

The authors declare no competing financial interest.

■ ACKNOWLEDGMENTS

This work was solely supported by the Center for Catalytic Hydrocarbon Functionalization, an Energy Frontier Research Center, funded by the U.S. Department of Energy, Office of Science, Office of Basic Energy Sciences, under Award DE-SC0001298.

■ REFERENCES

(1) Olah, G. A., Molnar, A., Eds. *Hydrocarbon Chemistry*, 2nd ed.; John Wiley & Sons: Hoboken, NJ, 2003.

(2) Labinger, J. A. *J. Mol. Catal. A: Chem.* **2004**, *220*, 27−35.

(3) Periana, R. A.; Bhalla, G.; Tenn, W. J., III; Young, K. J. H.; Liu, X. Y.; Mironov, O.; Jones, C.; Ziatdinov, V. R. *J. Mol. Catal. A: Chem.* **2004**, *220*, 7−25.

(4) Olah, G. A., Ed. *Beyond Oil and Gas: The Methanol Economy*; Wiley-VCH: Weinheim, Germany, 2006.

(5) International Energy, 2013, EIA Naturalgas.org, http://www.naturalgas.org/overview/resources.asp (accessed 10/2/13).

(6) Elvidge, C. D.; Ziskin, D.; Baugh, K. E.; Tuttle, B. T.; Ghosh, T.; Pack, D. W.; Erwin, E. H.; Zhizhin, M. *Energies* **2009**, *2*, 595−622.

(7) Arndtsen, B. A.; Bergman, R. G.; Mobley, T. A.; Peterson, T. H. *Acc. Chem. Res.* **1995**, *28*, 154−162.

(8) Carsch, K. M.; Cundari, T. R. *Comput. Theor. Chem.* **2012**, *980*, 133−137.

(9) Webb, J. R.; Bolano, T.; Gunnoe, T. B. *ChemSusChem* **2011**, *4*, 37−49.

(10) Schulz, H. *Appl. Catal., A* **1999**, *186*, 3−12.

(11) Goldberg, K. I.; Goldman, A. S. *ACS Symp. Ser.* **2004**, *885*, American Chemical Society: Washington, DC, pp 1−46.

(12) Perez, P. J. *Alkane C−H Activation by Single-site Metal Catalysis*; Springer: Berlin, 2012 .

(13) Stahl, S.; Labinger, J. A.; Bercaw, J. E. *Angew. Chem., Int. Ed.* **1998**, *37*, 2180−2192.

(14) Conley, B. L.; Tenn, W. J., III; Young, K. J. H.; Ganesh, S. K.; Meier, S. K.; Ziatdinov, V. R.; Mironov, O.; Oxgaard, J.; Gonzales, J.; Goddard, W. A., III; Periana, R. A. *J. Mol. Catal. A: Chem.* **2006**, *251*, 8−23.

(15) Blanksby, S.; Ellison, G. B. *Acc. Chem. Res.* **2003**, *36*, 255−263.

(16) Hoyano, J. K.; Graham, W. A. *J. Am. Chem. Soc.* **1982**, *104*, 3725−3727.

(17) Bergman, R. G. *Science* **1984**, *223*, 902−908.

(18) Jones, W. D.; Feher, F. J. *J. Am. Chem. Soc.* **1982**, *104*, 4240−4242.

(19) Desrosiers, P. J.; Shinomoto, R. S.; Flood, T. C. *J. Am. Chem. Soc.* **1986**, *108*, 1346−1347.

(20) Baker, M. V.; Field, L. D. *Organometallics* **1986**, *5*, 821−823.

(21) Crabtree, R. H. *J. Organomet. Chem.* **2004**, *689*, 4083−4091.

(22) Periana, R. A.; Taube, D. J.; Gamble, S.; Taube, H.; Satoh, T.; Fujii, H. *Science* **1998**, *280*, 560−564.

(23) Shilov, A. E.; Shulpin, G. B. *Chem. Rev.* **1997**, *97*, 2879−2932.

(24) Jones, C.; Taube, D.; Ziatdinov, V.; Periana, R.; Nielsen, R.; Oxgaard, J.; Goddard, W. *Angew. Chem.* **2004**, *116*, 4726−4729.

(25) Strassner, T.; Muehlhofer, M.; Zeller, A.; Herdtweck, E.; Herrmann, W. A. *J. Organomet. Chem.* **2004**, *689*, 1418−1424.

(26) Sen, A.; Benvenuto, M. A.; Lin, M.; Hutson, A. C.; Basickes, N. *J. Am. Chem. Soc.* **1994**, *116*, 998−1003.

(27) Kao, L.; Hutson, A. C.; Sen, A. *J. Am. Chem. Soc.* **1991**, *113*, 700−701.

(28) Palkovits, R.; Antonietti, M.; Kuhn, P.; Thomas, A.; Schuth, F. *Angew. Chem., Int. Ed.* **2009**, *48*, 6909−6912.

(29) Arndtsen, B. A.; Bergman, R. G. *Science* **1995**, *270*, 1970−1973.

(30) Janowicz, A. H.; Bergman, R. G. *J. Am. Chem. Soc.* **1983**, *105*, 3929−3939.

(31) Burger, P.; Bergman, R. G. *J. Am. Chem. Soc.* **1993**, *115*, 10462−10463.

(32) Negishi, E.; Van Horn, D. E.; Yoshida, T.; Rand, C. L. *Organometallics* **1983**, *2*, 563−565.

(33) Labinger, J. A.; Bercaw, J. E. *Nature* **2002**, *417*, 507−514.

(34) Kloek, S. M.; Heinekey, D. M.; Goldberg, K. *Angew. Chem., Int. Ed.* **2007**, *119*, 4820−4822.

(35) Kalman, S. E.; Petit, A.; Gunnoe, T. B.; Ess, D. H.; Cundari, T. R.; Sabat, M. *Organometallics* **2013**, *32*, 1797−1806.

(36) DeYonker, N.; Foley, N.; Cundari, T. R.; Gunnoe, T. B.; Peterson, J. *Organometallics* **2007**, *26*, 6604−6611.

(37) Figg, T. M.; Cundari, T. R.; Gunnoe, T. B. *Organometallics* **2011**, *30*, 3779−3785.

(38) Matsunaga, P. T.; Hillhouse, G. L.; Rheingold, A. L. *J. Am. Chem. Soc.* **1993**, *115*, 2075−2077.

(39) Figg, T. M.; Cundari, T. R. *Organometallics* **2012**, *31*, 4998−5004.

(40) Gunnoe, T. B. *Eur. J. Inorg. Chem.* **2007**, *9*, 1185−1203.

(41) Matsunaga, P. T.; Mavropoulos, J. C.; Hillhouse, G. L. *Polyhedron* **1995**, *14*, 175−185.

(42) Abu-Omar, M. M.; Espenson, J. H. *Organometallics* **1996**, *15*, 3543−3549.
(43) Abu-Omar, M. M.; Espenson, J. H. *J. Am. Chem. Soc.* **1995**, *117*, 272−280.
(44) Bischof, S. M.; Cheng, M.; Nielsen, R.; Gunnoe, T. B.; Goddard, W., III; Periana, R. *Organometallics* **2011**, *30*, 2079−2082.
(45) Gonzales, J.; Distasio, R.; Periana, R.; Goddard, W.; Oxaard, J. *J. Am. Chem. Soc.* **2007**, *129*, 15794−15804.
(46) Mei, J.; Carsch, K. M.; Freitag, C. R.; Gunnoe, T. B.; Cundari, T. R. *J. Am. Chem. Soc.* **2013**, *135*, 424−435.
(47) Figg, T. M.; Webb, J. R.; Cundari, T. R.; Gunnoe, T. B. *J. Am. Chem. Soc.* **2012**, *134*, 2332−2339.
(48) Brown, S.; Mayer, J. *J. Am. Chem. Soc.* **1996**, *118*, 12119−12133.
(49) Olatunji-Ojo, O. A.; Cundari, T. R. *Inorg. Chem.* **2013**, *52*, 8106−8113.
(50) Brown, S.; Myers, A.; Fulton, R.; Mayer, J. *Organometallics* **1998**, *17*, 3364−3374.
(51) Pouy, M. J.; Milczek, E. M.; Figg, T. M.; Otten, B. M.; Prince, B. M.; Gunnoe, T. B.; Cundari, T. R.; Groves, J. T. *J. Am. Chem. Soc.* **2012**, *134*, 12920−12923.
(52) Webb, J. R.: Burgess, S. A.; Cundari, T. R.; Gunnoe, T. B. *Dalton Trans.* **2013**, *42*, 16646−16665.
(53) Abu-Omar, M. M.; Hansen, P. J.; Espenson, J. H. *J. Am. Chem. Soc.* **1996**, *118*, 4966−4974.
(54) Conley, B. L.; Ganesh, S. K.; Gonzales, J. M.; Tenn, W. J., III; Young, K. J. H.; Oxgaard, J.; Goddard, W. A., III; Periana, R. A. *J. Am. Chem. Soc.* **2006**, *128*, 9018−9019.
(55) Asselt, A.; Trimmer, M. S.; Henling, L. M.; Bercaw, J. E. *J. Am. Chem. Soc.* **1988**, *110*, 8254−8255.
(56) Harvey, J. N. *Wiley Interdiscip. Rev.: Comput. Mol. Sci.* **2013**.
(57) Poli, R.; Harvey, J. N. *Chem. Soc. Rev.* **2003**, *32*, 1−8.
(58) Ni, C.; Power, P. *Chem. Commun.* **2009**, 5543−5545.
(59) Frisch, M. J. et al. *Gaussian 09*, revision B.01; Gaussian, Inc.: Wallingford, CT, 2009.
(60) Stevens, W. J.; Basch, H.; Krauss, M. J. *J. Chem. Phys.* **1992**, *70*, 612−630.
(61) Renz, M.; Bernard, M. *Eur. J. Org. Chem.* **1999**, *4*, 737−750.
(62) Brown, S.; Mayer, J. *J. Am. Chem. Soc.* **1994**, *116*, 2219−2220.
(63) Brown, S.; Mayer, J. *Organometallics* **1995**, *14*, 2951−2960.
(64) Bassetti, M.; Sunley, G. J.; Maitlis, P. M. *J. Chem. Soc., Chem. Commun.* **1988**, 1012−1013.
(65) Webb, J. R.; Figg, T. M.; Otten, B. M.; Gunnoe, T. B.; Cundari, T. R.; Sabat, M. *Eur. J. Inorg. Chem.* **2013**, 4515−4525.
(66) Groves, J. T.; Bonchio, M.; Carofiglio, T.; Shalyaev, K. *J. Am. Chem. Soc.* **1996**, *118*, 8961−8962.
(67) Cooper, H. L.; Groves, J. T. *Arch. Biochem. Biophys.* **2011**, *507*, 111−118.
(68) Groves, J. T. *J. Inorg. Biochem.* **2006**, *100*, 434−447.
(69) Ess, D. H.; Gunnoe, T. B.; Cundari, T. R.; Goddard, W. A.; Periana, R. A. *Organometallics* **2010**, *29*, 6801−6815.
(70) Smeltz, J. L.; Webster, C. E.; Ison, E. A. *Organometallics* **2012**, *31* (10), 4055−4062.
(71) Holm, R.; Donahue, J. *Polyhedron* **1993**, *12*, 571−589.
(72) Koo, K.; Hillhouse, G. L.; Rheingold, A. L. *Organometallics* **1995**, *14*, 456−460.